Research Square

Preprints are preliminary reports that have not undergone peer review.
They should not be considered conclusive, used to inform clinical practice,
or referenced by the media as validated information.

# The Structural, Magnetic and Optical Properties of Ni-Mg-Zn Ferrite Prepared With Different Complexing Agents via Sol-Gel Method

**Yanchun Zhang**
Northwest Normal University
**Aimin Sun** ( Aiminsun_1138@163.com )
Northwest Normal University https://orcid.org/0000-0002-6099-652X
**Zhaxi Suonan**
Northwest Normal University

**Research Article**

**Keywords:** Ni-Mg-Zn ferrite, sol-gel method, soft magnetic material, different complexing agents.

**Posted Date:** March 4th, 2021

**DOI:** https://doi.org/10.21203/rs.3.rs-263070/v1

**License:** This work is licensed under a Creative Commons Attribution 4.0 International License.
Read Full License

**Version of Record:** A version of this preprint was published at Journal of Materials Science: Materials in Electronics on April 19th, 2021. See the published version at https://doi.org/10.1007/s10854-021-05914-6.

# The structural, magnetic and optical properties of Ni-Mg-Zn ferrite prepared with different complexing agents via sol-gel method

Yanchun Zhang[1], Aimin Sun[1,2 *], Zhaxi Suonan[1]

1 College of Physics and Electronic Engineering, Northwest Normal University,

Lanzhou 730070, China

2 Key Laboratory of Atomic and Molecular Physics & Functional Materials of Gansu Province,

Lanzhou 730070, China

**Abstract:** Different complexing agents were used to prepare Ni-Mg-Zn ferrite with the composition formula $Ni_{0.2}Mg_{0.2}Zn_{0.6}Fe_2O_4$ via sol-gel method, which included citric acid, oxalic acid, egg white and EDTA. The $Ni_{0.2}Mg_{0.2}Zn_{0.6}Fe_2O_4$ ferrite with no complexing agent was also prepared as a comparison. The chemical phases of samples were analyzed by the X-ray diffraction (XRD), which indicated that samples had spinel phase structure. The lattice constants of samples are in the range of 8.3980~8.4089 Å. The composition and structure were further studied by fourier transform infrared spectroscopy (FTIR). There were two typical characteristic bands related to the stretching vibrations of spinel ferrite in FTIR spectra. Scanning electron microscope (SEM) micrographs and transmission electron microscope (TEM) images showed that the particles have the shape of spherical cube. Energy dispersive spectrometer (EDS) analyzed the elements and ingredients of samples, which included Ni, Mg, Zn, Fe and O. X-ray photoelectron spectroscopy (XPS) is used to examine further the elemental composition and chemical state of sample prepared with EDTA as complexing agent. The optical properties of samples were investigated by photoluminescence spectra and UV-Vis spectroscopy. Vibrating sample magnetometer (VSM) was used to characterize magnetic properties, hysteresis loops revealed the ferrimagnetism behavior of prepared samples.

**Keywords:** Ni-Mg-Zn ferrite; sol-gel method; soft magnetic material; different

* Corresponding Author: Aimin Sun AiminSun_1138@163.com

complexing agents.

## 1. Introduction

With the development of electronic industry and information technology, the demand for electronic equipment in the market is increasing and the requirements for electronic devices are more stringent. The field of soft magnetic nanomaterials flourishes with its excellent characteristics, which are widely used in magnetic resonance imaging, computer cores; magnetic shielding, electronic computer switching element and storage element [1-4].

Soft magnetic materials include soft ferrite, amorphous and nano-microcrystalline metallic soft magnetic materials, metallic soft magnetic materials. The low resistivity of metal soft magnetic material leads to skin effect, and eddy current loss limits its application in high frequency band. Amorphous and nano-crystalline metal soft magnetic materials are superior to ferrite in performance, but inferior in cost performance. Therefore, ferrite still dominates the market. Among the many ferrite types, spinel ferrites have always attracted much attention due to largely considerable properties they appeared, such as magnetic compensation behavior, spin glass behavior, critical behavior, etc. [5-7]. The lattice structure of spinel ferrite belongs to cubically symmetric and is densely packed with $O^{2-}$, cations fill the gaps where the $O^{2-}$ are densely packed. In the face-centered cubic lattice constituted by the accumulation of 32 $O^{2-}$, there are two kinds of gaps, namely tetrahedral A site and octahedral B site. Fig. 1 shows the crystal structure of spinel ferrite and the distribution of cations and $O^{2-}$. Some researchers doped cations or oxide (CuO, $Bi_2O_3$, etc.) in ferrite to modify the electrical and magnetic properties according to the large gap provided by the spinel structure [8-10]. The conditions of pH and annealing temperature also have effects on morphology and properties [11-13].

Among the many spinel ferrites, Ni-Zn ferrite is widely used in iron cores of transformers, magnetic heads and magnetic media for magnetic recording by virtue of the advantages such as low coercivity, high electrical resistivity [14]. $NiFe_2O_4$ is a sort of soft ferrite regarded as a collinear ferrimagnet [15]. $MgFe_2O_4$ is a kind of soft magnetic used in high density recording ferrofluids [16]. Ni-Mg-Zn ferrite has a broad

application prospect as a typical soft magnetic material with a small magnetocrystalline anisotropy constant. Many researchers synthesize ferrite with some conventional technology including electrospinning method, microwave method, rheological phase reaction method, sol-gel method, solid phase method, microemulsion method, mechanochemical reaction method, etc [17-25]. In all synthesis methods, the sol-gel method is one of the simple, cheap and versatile techniques, which quickens the synthesis of compounds, lets surface morphology fine and makes crystal homogeneity. When the sol-gel method is used to prepare ferrite, one thing worth noting is the choice of complexing agent. The complexing agent can effectively complex metal ions of different ion sizes and can also be used as a spontaneous combustion fuel. M.A. Gabal et al.[26] used egg white to prepare Ni-Zn ferrite and obtained a single phase structure. C. Choodamani et al.[27] used the mixture of sugar and urea as fuel to prepare Mg-Zn ferrite and had superparamagnetic particles in samples. Shaban I. Hussein et al.[28] used ethylenediamine tetraacetic acid to prepare $MgFe_2O_4$ and obtained large saturation magnetization (28.96 emu/g) annealing at 600 ℃.

It is curious to know whether there are some influences on Ni-Mg-Zn ferrite using different complexing agents via sol-gel method. Under the condition of well controlled annealing temperature and solution pH, it is an unprecedented work to prepare Ni-Mg-Zn ferrite via sol-gel method with different complexing agents. Hence, the effects of complexing agents on Ni-Mg-Zn ferrite were explored using sol-gel method in this work.

## 2. Experimental Process

### 2.1 Materials

High purity metal nitrates included nickel nitrate [$Ni(NO_3)_2 \cdot 6H_2O$], (Mw: 290.81 g/mol; 98%), magnesium nitrate [$Mg(NO_3)_2 \cdot 6H_2O$], (Mw: 256.41 g/mol; 99.0%), zinc nitrate [$Zn(NO_3)_2 \cdot 6H_2O$], (Mw: 297.49 g/mol; 99.0%), ferric nitrate [$Fe(NO_3)_3 \cdot 9H_2O$], (Mw: 404.00 g/mol; 98.5%), which mass were weigh with a laboratory balance by stoichiometric ratio. Different complexing agents contained citric acid ($C_6H_8O_7 \cdot H_2O$), oxalic acid ($C_2H_2O_4$), egg white, ethylenediamine tetraacetic acid (EDTA, $C_{10}H_{16}N_2O_8$), respectively.

## 2.2 Synthesis

The $Ni_{0.2}Mg_{0.2}Zn_{0.6}Fe_2O_4$ ferrite were prepared with sol-gel method using different complexing agents. As a comparison, the $Ni_{0.2}Mg_{0.2}Zn_{0.6}Fe_2O_4$ ferrite with no complexing agent was also prepared. The metal nitrates and oxalic acid, EDTA, citric acid were dissolved in 150 mL distilled water at a molar ratio of 1:1.2 in a clean beaker, respectively. The amount of fresh egg white is 20 mL, which mixed in 150 mL distilled water to prepare precursor solution. A glass rod was used to stir the solution in a fixed direction at a constant speed until the solute was completely dissolved into a clear state. The pH of solution was controlled around 7 by adding drops of ammonium hydroxide under the condition of uniform stirring. The precursor solution was heated at 80 ℃ for 3h in magnetic heating and stirring agitator until the solution turned to a wet sol. The wet sol was put in dry blast oven at 120 ℃ for 2h to form a dry gel. The dry gel was heated with an alcohol lamp to form gray floccule and the floccule was ground more evenly about 1h to get a black powder. The powders were calcined in muffle furnace at 950 ℃ for 2h. The annealed powders were ground about 20 min to obtain final samples which were used to characterize the properties. Fig. 2 is the flow chart of the experiment. The chemical process of this experiment can be written as:

$$\left.\begin{array}{l} 6H_2O + 2Ni(NO_3)_2 + 2Mg(NO_3)_2 + \\ +6Zn(NO_3)_2 + 20Fe(NO_3)_3 \end{array}\right\} + \left\{\begin{array}{c} \text{None} \\ \text{Citric acid} \\ \text{Oxalic acid} \\ \text{Egg white} \\ \text{EDTA} \end{array}\right\} + \xrightarrow{\text{Heat + Stir}}$$

$$\left\{ 10Ni_{0.2}Mg_{0.2}Zn_{0.6}Fe_2O_4 + 30NO_2\uparrow + 70O_2\uparrow + 10N_2\uparrow + 6H_2O\uparrow \right.$$

## 2.3 Characterization Techniques

The X-ray diffraction patterns were collected by Germany Bruch Diffractometer with a goniometer using Cu-Kα radiation ( λ=0.15406 nm ). The diffracted intensities were recorded in the angular range 20°~80°. The infrared absorption spectra of samples within the scope of 300cm$^{-1}$~4000 cm$^{-1}$ were recorded by China WQF-510 Fourier transform infrared spectroscopy. The phase and vibrational bands information were found. The morphology and shape were observed by scanning electron microscopy Japan JSM-6700F. Chemical elements of samples were tested by Japan JSM-6700F energy dispersive spectrometer. The elemental composition and chemical

state were examined further by X-ray photoelectron spectroscopy PHI5702 with excitation source of Al. The magnetic properties including Mr, Ms and Hc were obtained by using USA Lakeshore 7304 vibrating sample magnetometer. The UV-visible absorption spectrum were recorded by UV-Vis spectrophotometer (Japan, Hitachi U-3900H).

## 3. Results and Discussion

### 3.1 XRD analysis

The XRD patterns of the $Ni_{0.2}Mg_{0.2}Zn_{0.6}Fe_2O_4$ ferrite prepared with different complexing agents are shown in Fig.3(a). What can be seen from the pattern is that X-ray diffraction peaks of $Ni_{0.2}Mg_{0.2}Zn_{0.6}Fe_2O_4$ ferrite prepared by using different complexing agents contain 9 main characteristic peaks, which are (111), (220), (311), (222), (400), (422), (511), (440) and (533). $Ni_{0.2}Mg_{0.2}Zn_{0.6}Fe_2O_4$ ferrite prepared with citric acid have the sharpest peaks, the peaks (311) of other samples are also quite obvious. It can be preliminarily inferred from the characteristic peak that the prepared samples have spinel phase structure. Figure 3(b) shows a contrast between XRD pattern of samples ( prepared with egg white and EDTA) and the JCPDS card #00-086-2267 for $NiFe_2O_4$ which belongs to spinel system with space group Fd3m. The spinel phase structure of the samples are confirmed.

Parameters derived from XRD data consisting of inter-planar spacing (d), lattice constant ($a$), average crystallite sizes (D), dislocation linear density (δ) and X-ray density ($\rho_x$) are displayed in Table 1. The inter-planar spacing (d) is calculated with Bragg condition. The formula is shown below:

$$n\lambda = 2d\sin\theta \tag{1}$$

Where 'n' is X-ray diffraction series, 'λ' is the wavelength of X-ray (0.15406 nm), 'θ' is the diffraction angle. The lattice constant ($a$) is obtained by using the equation below [29]:

$$a = \lambda\sqrt{\left(h^2 + k^2 + l^2\right)}/2\sin\theta \tag{2}$$

The (h k l) are Miller index. The average crystallite size (D) of the samples are calculated from the most intense (311) peak of XRD by the classic Scherrer's formula. The formula is as follows [30]:

$$D_{Scherrer} = 0.9\lambda/\left(\beta\cos\theta\right) \tag{3}$$

Where 0.9 is shape factor; β is the full width at half maximum of the diffraction angle abbreviated as FWHM. The average crystallite size ($D_{W-H}$) and internal strains (ε) of the samples can be obtained by the Williamson-Hall method:

$$\beta\cos\theta = \frac{k\lambda}{D_{W-H}} + 4\varepsilon\sin\theta \tag{4}$$

The above relationship can be regarded as a linear function ($y=A+Bx$). Internal strains (ε) can be expressed by the slope of this line. In Williamson-Hall Method, the average crystallite size is calculated from full width at half maximum (FWHM) of the peaks (111), (220), (311), (222), (400), (422), (511), (440) and (533). The W-H plot of sample prepared with citric acid showed negative strain, which may be attributed to lattice shrinkage [31]. The plot of (4sinθ, βcosθ) for samples are shown in Fig.4. The average crystallite size ($D_{W-H}$) obtained by W-H method is presented in Table 1. Compared with the Scherrer method, the W-H method has an advantage in taking strain into account. At the same time, the W-H method has a less weight on data from higher angles. The dislocation line density (δ) of the prepared samples are given by the following formula [32]:

$$\delta = 1/D_{Scherrer}^2 \tag{5}$$

The X-ray density ($\rho_x$) can be calculated with the equation below [33]:

$$\rho_x = \frac{8M}{N_A a^3} \tag{6}$$

Where 'M' is the molecular mass of the sample (231.53 g/mol); '$N_A$' is the Avogadro's constant and the value is $6.02214076\times10^{23}$ $mol^{-1}$.

In Table 1, the lattice constants of prepared $Ni_{0.2}Mg_{0.2}Zn_{0.6}Fe_2O_4$ samples are in the range of 8.3980~8.4089 Å. The average crystallite sizes ($D_{Scherrer}$) of these samples are different from each other. The order from small to large is citric acid (53.11 nm), egg white (60.86 nm), EDTA (65.14 nm), oxalic acid (68.91 nm), none (68.91 nm). Dislocation line density (δ) is related to lattice defects, the δ value of sample is smaller, the defect density is lower and the crystallinity is higher [34]. The X-ray density ($\rho_x$) of samples are also shown in Table 1.

### 3.2 FTIR analysis

When a molecule is irradiated with infrared light, the chemical bonds or functional groups in the molecule can vibrate and absorb. Different molecules have a unique infrared absorption spectrum on account of its composition and structure. Fig. 5 is the FTIR spectra of the $Ni_{0.2}Mg_{0.2}Zn_{0.6}Fe_2O_4$ ferrite prepared with different complexing agents. In accordance with Waldron [35], the high frequency absorption bands marked as $\nu_1$ at around 600 $cm^{-1}$ is relevant to the tetrahedral metal vibration, which is strong stretching vibration. And the low frequency absorption bands marked as $\nu_2$ at around 400 $cm^{-1}$ is corresponding to the octahedral metal vibration which is regarded as weak stretching vibration. It can be found that there are absorption bands $\nu_1$ and $\nu_2$ in Fig.5. And the frequency values of $\nu_1$ and $\nu_2$ are recorded in Table 2. The absorption bands $\nu_1$ of the prepared samples are in the range of 597 $cm^{-1}$~609 $cm^{-1}$ and the absorption bands $\nu_2$ are between 397 and 414 $cm^{-1}$. The existence of band at 1635 $cm^{-1}$ may be due to the stretching vibration of the -OH bond of remaining water molecule [34]. The band at 1384 $cm^{-1}$ is seen as the vibration of $NO_3^-$ bond, the decrease or disappearance of the band at 1384 $cm^{-1}$ can indicate that $NO_3^-$ participated in the process of reaction [36]. The absorption bands located at 1110 $cm^{-1}$ may be related to the existence of remaining C-O bands. From the FTIR spectra, it can be inferred that the prepared samples have spinel structure which is in conformity with the result of the XRD analysis.

### 3.3 Morphological analysis

#### 3.3.1 SEM analysis

The surface morphology and particles size distribution histograms of the $Ni_{0.2}Mg_{0.2}Zn_{0.6}Fe_2O_4$ ferrite prepared with different complexing agents are shown in Fig.6. Evidently, it can be observed that particles prepared with different complexing agents have the shape of spherical cube. The particles prepared with citric acid as complexing agents are relatively uniform. The particles prepared with egg white and oxalic acid as complexing agent are uneven in size. It can be seen that the particles of the sample using egg white as the complexing agent are sharp and angular from Fig.6. From particles size distribution histogram of samples, it was found that the average particles size of sample prepared with oxalic acid is 188 nm, which is bigger than other samples. There are cluster phenomenons among prepared particles, which is

attributed to the high annealing temperature. The interaction of spin coupling between magnetic ions can also cause particles to adhere to each other [37]. That's why the sample has a larger particle size.

### 3.3.2 TEM analysis

Fig. 7(a) and (b) are TEM images of $Ni_{0.2}Mg_{0.2}Zn_{0.6}Fe_2O_4$ ferrite prepared with EDTA. Owing to magnetostatic coupling, the phenomenon of highly agglomerated particles was presented. Figure 7(c) is the selected area electron diffraction (SAED) image of sample prepared with EDTA as complexing agent. It can be seen the diffraction rings related to the diffraction peaks of spinel ferrite.

## 3.4 Chemical elements analysis

Energy dispersive spectrometer is used to analyze chemical elements and ingredients in $Ni_{0.2}Mg_{0.2}Zn_{0.6}Fe_2O_4$ ferrite prepared with different complexing agents. The EDS diagrams of prepared samples are shown in Fig.8. It can be found that the main elements of the $Ni_{0.2}Mg_{0.2}Zn_{0.6}Fe_2O_4$ ferrite prepared with different complexing agents are Ni, Mg, Zn, Fe and O. Some researchers used egg white as a complexing agent to prepare ferrite and found that the sample contained S, Cl and K elements, which are all trace elements contained in egg white [34]. In this experiment, S, Cl and K elements also exist in the sample prepared with egg white as complexing agent. Considering that S, Cl and K belong to impurity elements, the elements are not marked in the figure but exist in 2~4 keV.

## 3.5 XPS study

Different atoms have a unique binding energy related to the chemical state of the atom and the molecular environment, when the cations are distributed in A and B sites of ferrite. XPS technique was performed to discover the elemental composition and state in prepared spinel ferrite. The XPS spectrum of $Ni_{0.2}Mg_{0.2}Zn_{0.6}Fe_2O_4$ ferrite prepared with EDTA as complexing agent was displayed in Fig.9. It can be seen that there are the binding energy peaks of Ni, Mg, Zn, Fe, O and C from Fig.9(a). It is inevitable that carbon element appears in the spectrum as an impurity element during the measurement process. Ni, Mg, Zn, Fe and O are the main elements related to this experiment. The XPS core level spectrum about Ni 2p, Mg 2p, Zn 2p, Fe 2p and O 1s of prepared $Ni_{0.2}Mg_{0.2}Zn_{0.6}Fe_2O_4$ ferrite with EDTA were shown in Fig.9(b)-(f). The

doublets of Ni $2p_{1/2}$ and Ni $2p_{3/2}$ located at 872.4 and 854.9 eV. The Ni $2p_{3/2}$ in the sample is less than that of $NiFe_2O_4$ (855.1 eV) [38]. One peaks at 55.4 eV is related to the binding energy of Mg 2p, which reveals Mg element existed in sample [39]. Two distinct peaks at 1021.1 and 1044.2 eV corresponding to Zn $2p_{3/2}$ and Zn $2p_{1/2}$ are seen from Fig.9(d) [40]. As far as Fe 2p is concerned, the peak located at 725.0 and 711.3 eV associated with Fe $2p_{1/2}$ and Fe $2p_{3/2}$ [41]. Simultaneously, the satellite peak of $Fe^{3+}$ can be observed at 720.0 eV. The relative contributions to the overall intensity of $Fe^{3+}$ ions at A and B sites are 40.27% and 59.73%, respectively, which can be obtained by the area occupied by the two fitted peaks [34]. The core level spectrum of O 1s is shown in Fig.9(f), in which there are two peaks appearing corresponding to two different oxides. The peak at 531.0 eV relates to surface oxygen components and the peak at 529.7 eV is in touch with lattice $O^{2-}$ [42]. It can summarize from XPS analysis that Ni, Mg, Zn and Fe exist at its opportune valence in $Ni_{0.2}Mg_{0.2}Zn_{0.6}Fe_2O_4$ ferrite prepared with EDTA as complexing agent.

**3.6 Cation distribution**

In reverse spinel ferrite, 8 divalent metal ions locate at B site, while 16 $Fe^{3+}$ ions occupy evenly both A and B sites. Based on Néel two sublattice models, the cation distribution formula as follow [43]:

$$\left(Fe^{3+}\right)_A\left\{Me^{2+}Fe^{3+}\right\}_B O_4 \tag{7}$$

Mossbauer spectroscopy of bulk $NiFe_2O_4$ reveals anti-spinel structure [44]. There is a strong tendency of $Ni^{2+}$ to occupy the B site. $Fe^{3+}$ ions tend to occupy A and B sites. By consulting relevant reference [45], the ionic fraction of $MgFe_2O_4$ is $(Mg_{0.1}Fe_{0.9})_A[Mg_{0.9}Fe_{1.1}]_BO_4$. More $Mg^{2+}$ ions tend strongly to occupy B site. It is due to a strong tendency to occupy A site for $Zn^{2+}$ ions, $ZnFe_2O_4$ has a normal spinel structure. The cation distribution of prepared $Ni_{0.2}Mg_{0.2}Zn_{0.6}Fe_2O_4$ ferrite can be described as:

$$\left(Zn_{0.6}^{2+}Fe_{0.4}^{3+}\right)_A\left\{Ni_{0.2}^{2+}Mg_{0.2}^{2+}Fe_{1.6}^{3+}\right\}_B O_4 \tag{8}$$

According to the cation distribution of $Ni_{0.2}Mg_{0.2}Zn_{0.6}Fe_2O_4$ ferrite, the average ion radius and oxygen parameters at B site can be calculated by the following formula [46]:

$$r_B = \frac{1}{2}\left\{0.2r_{Ni^{2+}} + 0.2r_{Mg^{2+}} + 1.6r_{Fe^{3+}}\right\} \quad (9)$$

$$u = \frac{5}{8} - \frac{\left(r_B + r_0\right)}{a} \quad (10)$$

Where '$a$' is the lattice constant, '$r_0$' is the radius of $O^{2-}$ (0.140 nm), the radius of $Ni^{2+}$ is 0.072 nm, the radius of $Mg^{2+}$ is 0.065 nm, the radius of $Zn^{2+}$ is 0.074 nm, the radius of $Fe^{3+}$ is 0.064 nm. The values of '$r_B$' and 'u' are given in Table 3. Figure 10 shows the relative positions of cations and $O^{2-}$ in the superexchange of spinel ferrite. The distances between cations and anions (Me-O: p, q, r and s) and the distances between cations (Me-Me: b, c, d, e and f) can be calculated by Eqs. (11) and (12) [47].

$$p = a\left(\frac{1}{2} - u\right) \quad q_r = \sqrt{3}a\left(u - \frac{1}{8}\right) \quad s = \frac{\sqrt{3}}{3}a\left(u + \frac{1}{2}\right) \quad r = \sqrt{11}a\left(u - \frac{1}{8}\right) \quad (11)$$

$$b = \frac{\sqrt{2}}{4}a \quad c = \frac{\sqrt{11}}{8}a \quad d = \frac{\sqrt{3}}{4}a \quad e = \frac{3\sqrt{3}}{8}a \quad f = \frac{\sqrt{6}}{4}a \quad (12)$$

The experimental values of lattice constant 'a' and oxygen parameter 'u' are used to calculate the distance between ions (Me-O and Me-Me). The values of these distances about samples prepared with different complexing agents are shown in Table 3. The 'b' and 'd' are related to the distances (jump length) between magnetic ions at B and A sites. The distance between cation and oxygen ion at A site and B site are '$q_r$' and 'p'. It can be seen from Table 3 that the values of these distances have similar behavior to the lattice constant. The lattice constant is related to the cation radius and the cation distribution in spinel structure. Due to different complexing agents used, the distances between ions of the prepared samples are different. The sample prepared with EDTA has a bigger $q_r$ value and a lower p value. It can be due to the transformation that some $Mg^{2+}$ ions with bigger ion radius enter into A site from B site and replace some original $Fe^{3+}$ ions with smaller ion radius at A site in the sample prepared with EDTA. Thereby, the distances between ions are different.

### 3.7 Magnetic properties study

Magnetic properties are crucial properties of ferrite, which relate to microstructure (such as grain size, grain uniformity, sintering compactness), chemical composition, preparation method, types of metal ions, cation distribution etc.

Magnetic materials have obvious response to external magnetic field, which can be characterized by hysteresis loops. The magnetic characterization of $Ni_{0.2}Mg_{0.2}Zn_{0.6}Fe_2O_4$ ferrites prepared with sol-gel method using different complexing agents are carried out at room temperature with the applied field range of ±12 kOe. The hysteresis loops of the prepared samples are shown in Fig.11 (a). It shows from hysteresis loops that prepared samples are typical soft magnetic materials. The magnetism of cubic spinel ferrite mainly comes from metal cation superexchange between A and B sites. There is no direct cation exchange in A and B sites. Superexchange can be achieved through $O^{2-}$ as media. There are three types of superexchange. Taking into account factors such as the superposition probability of the electron wave function, A-B type plays the most important role, A-A type and B-B type are relatively weak.

The parameters related to magnetism are displayed in Table 4 and Table 5. Using different complexing agents makes a great difference to magnetic properties of $Ni_{0.2}Mg_{0.2}Zn_{0.6}Fe_2O_4$ ferrite. It can learn from Table 3 that remanent magnetization of prepared samples from small to large are 0.1102, 0.1556, 0.5432, 1.0643 and 1.8003 emu/g corresponding to oxalic acid, none, citric acid, egg white and EDTA, respectively. Saturation magnetization are 26.47, 29.06, 30.11, 32.20 and 38.25 emu/g for using oxalic acid, citric acid, egg white, none and EDTA, respectively. The values of coercivity are 2.480, 2.522, 4.866, 11.746 and 12.027 Oe with the order of complexing agent: none, oxalic acid, citric acid, egg white and EDTA. The solubility of EDTA is low when the pH of solution is low. It can be further dissolved in the process of adjusting the pH by adding ammonium hydroxide. EDTA and ammonium hydroxide compete to complex metal ions, which leads to uneven distribution of metal ions in dry gel prepared with EDTA. So the sample prepared with EDTA has a bigger Hc than other samples. In the process of preparing the sample with egg white, $Fe^{3+}$ ions first react with $OH^-$ to form yellow precipitation when the pH of solution is adjusted by adding ammonium hydroxide, then egg white react with the yellow precipitation and make it dissolved. Meanwhile, the complex constant of egg white is lower, it also lead to uneven distribution of metal ions. The sample prepared with egg white had the second biggest coercivity among all samples. It is significant to declare

that due to the prepared samples have low coercivity, it has a broad development prospect on magnetic recording applications [48]. Fig.11 (b) shows a larger view of the first quadrant in hysteresis loops. The value of squareness S (Mr/Ms) and coercivity squarenes S* are displayed in Table 4, which is a significant parameter about anisotropy. Very small values appeared on Mr/Ms of prepared samples revealed that -ve dipolar interactions occupy a dominant position in remanance state. Meanwhile, due to the appearance of -ve dipolar interactions, it can prove that there are superparamagnetic particles existed in prepared samples [28,48].

On the basis of Néel theory [49], it is significant to declare that due to antiparallel couping between A and B sites in spinel structured ferrite, the remaining spontaneous magnetization is generated. The ferrimagnetism showed by prepared Ni-Mg-Zn ferrite derives from the antiparallel couping of magnetic moment between $Ni^{2+}$ ion ($2\mu_B$) at B site and $Fe^{3+}$ ion ($5\mu_B$) at A site. In addition, $Mg^{2+}$ ion and $Zn^{2+}$ ion all have magnetic moment of $0\mu_B$, which have no unpaired electrons. The net magnetization of each formula unit can be expressed as follows [50]:

$$\mu_B(Cal.) = M_B - M_A \tag{13}$$

In which $M_B$ and $M_A$ are the magnetic moments of B and A sites, respectively. Meanwhile, the Bohr magnetic moment can be calculated with the formula [51]:

$$\mu_B(\exp.) = \frac{M_W \times M_S}{5585} \tag{14}$$

Where 'Mw' is the molecular weight. The value of unit cell magnetic moment $\mu_B$(exp.) is shown in Table 5. The magnetic moment each formula unit can be also obtained by Yafet-Kittle three sub-lattice model,which express as follow[52]:

$$\mu_B(\exp) = M_B \cos\alpha_{YK} - M_A \tag{15}$$

The Y-K($\alpha_{YK}$) can be obtained by the formula:

$$\cos\alpha_{YK} = \frac{\mu_B(\exp) + M_A}{M_B} \tag{16}$$

$M_B$ and $M_A$ are the magnetic moment of B and A sites in $(Zn_{0.6}Fe_{0.4})_A[Ni_{0.2}Mg_{0.2}Fe_{1.6}]_B$

$M_A = (0.6\times 0 + 0.4\times 5)\mu B = 2\mu B$

$M_B = (0.2\times 2 + 0.2\times 0 + 1.6\times 5)\mu B = 8.4\mu B$

The values of $\alpha_{YK}$ are shown in Table 5. The largest saturation magnetization corresponds to the smallest $\alpha_{YK}$. The coercivity is the strength of the reverse magnetic

field that needs to be applied to reduce the magnetization to zero. The coercivity can be expressed by the following Brown's relation [49]:

$$Hc = \frac{2K}{\mu_0 \times Ms} \tag{17}$$

Among them, 'K' represents anisotropy constant, '$\mu_0$' is magnetic permeability in vacuum and the value is 1 in Gaussian. The value of anisotropy constant is displayed in Table 5. The magnetic moment $\mu_B$(exp.) of prepared $Ni_{0.2}Mg_{0.2}Zn_{0.6}Fe_2O_4$ ferrite with different complexing agents are 1.09 (oxalic acid), 1.20 (citric acid), 1.24 (egg white), 1.33 (none) and 1.58 (EDTA), respectively. The anisotropy constant are 2.30 (EDTA), 1.76 (egg white), 0.70 (citric acid ), 0.39 (none) and 0.33 (oxalic acid) in $10^2$ erg/g. The magnetization and the external magnetic field have the following relationship:

$$M = \chi H \tag{18}$$

Where '$\chi$' is magnetic susceptibility. Magnetic susceptibility of ferrimagnetism have the order of magnitude of $10^0$~$10^3$, which is smaller than that of ferromagnetism. The magnetization of soft ferrite mainly depend on the rotation of the magnetic moment of magnetic domain in the direction of the magnetic field, which also named the magnetic rotation [43]. Magnetic susceptibility '$\chi$' can also be expressed by the field dependence of dM/dH curves, which characterize the feature of domain about prepared samples. The field dependence of dM/dH curves of prepared $Ni_{0.2}Mg_{0.2}Zn_{0.6}Fe_2O_4$ ferrite with different complexing agents are shown in Fig.12. The dM/dH values at H→0 of the prepared samples with different complexing agents are 41.53 (oxalic acid), 58.77 (none), 79.91 (egg white), 95.66 (citric acid) and 123.25 (EDTA) in $10^{-3}$ emu/g Oe. It reveals that pseudo-single domain, single domain, and multi-domain of the prepared samples [53]. The dM/dH values at H→Hm of the prepared samples are 42.67 (oxalic acid), 61.31 (none), 90.51 (egg white), 107.07 (citric acid) and 148.86 (EDTA) in $10^{-3}$ emu/g Oe. It should be pointed out that Hc values of prepared samples are less than Hm values on account of the switching field distribution [43].

### 3.8 Optical studies

#### 3.8.1 Photoluminescence spectra

The photoluminescence spectroscopy is an important technique for studying optical properties and obtaining information about band gap defect states of spinel structure in semiconducting materials [54]. In spinel structure ferrite, due to cation disorder, there are many defects, which can be regarded as electron or hole traps [55]. Moreover, the PL spectrum nature of $Ni_{0.2}Mg_{0.2}Zn_{0.6}Fe_2O_4$ spinel ferrite depends on the complexing agents used in sol-gel method. Figure 13 shows the room temperature PL spectra of $Ni_{0.2}Mg_{0.2}Zn_{0.6}Fe_2O_4$ spinel ferrite prepared with none, egg white and EDTA recorded at the excitation wavelength ($\lambda_{ex}$) of 325 nm. The PL spectrum can be assigned to the charge transfer between cation and its surrounding oxygen ions in tetrahedral and octahedral sites. As can be seen from the spectra, the prepared $Ni_{0.2}Mg_{0.2}Zn_{0.6}Fe_2O_4$ spinel ferrite nanoparticles show broad intrinsic emission peaks in the range of 330~560 nm and the sample prepared without complexing agent has the highest luminescence intensity at 380~560 nm. The obtained PL spectra show strong violet (400~450 nm), blue (450~490 nm), green (490~560 nm) emission bands in the visible region and UV (300~380 nm). The violet emission band observed around 441 nm (none, 2.81 eV), 436 nm (EDTA, 2.84 eV) and 428 nm (egg white, 2.89 eV) attributed to emission from some deep level in the band gap [56]. The blue emission may be due to the radiative defects related to the interface traps existing at the grain boundaries [57]. The green emission may be related to the recombination of electrons deeply trapped in oxygen vacancies with photo-generated holes [58]. A strong UV emission band at 340 nm (EDTA, 3.64 eV), 340 nm (egg white, 3.64 eV) and 345 nm (none, 3.59 eV) may be due to the quantum confinement effect which broadens the band gap [56].

**3.8.2 UV-Visible analysis**

The optical properties of $Ni_{0.2}Mg_{0.2}Zn_{0.6}Fe_2O_4$ spinel ferrite prepared with none and EDTA are analyzed by using diffuse reflectance UV-Visible spectrophotometer. Figure 14 shows UV-Vis absorption spectrum of samples prepared with none and EDTA as complexing agents.The optical band gap energy ($E_g$) can be estimated by the Tauc's relation [57]:

$$(\alpha h\nu)^{\frac{1}{n}} = A(h\nu - E_g) \tag{19}$$

Where '$\alpha$' is the absorption coefficient, '$h$' is Planck's constant, '$h\nu$' is the photon

energy, '*A*' is a proportionality constant. The value of 'n' depends on the electronic transitions type of semiconductor. When 'n' is 1/2, it is direct optical transition; when 'n' is 2, it is indirect optical transition. Figure 15 reflects the Tauc plots of the samples prepared with none and EDTA. A Tauc plot of $(\alpha h\nu)^{1/2}$ versus photon energy ($h\nu$) was drawn to estimate the value of indirect band gap. The optical band gap energy can be obtained by extrapolaing the linear portion when '$\alpha$' is 0. The band gap value are 1.68 and 1.65 eV for samples prepared with none and EDTA, respectively.

## 4. Conclusions

$Ni_{0.2}Mg_{0.2}Zn_{0.6}Fe_2O_4$ spinel ferrite were prepared using sol-gel method with none, citric acid, oxalic acid, egg white, EDTA as complexing agents. XRD analysis showed all the major peaks related to spinel structure without extra peak intensity. The FTIR spectra at room temperature displayed two main absorption bands corresponding to complexes at A and B sites in spinel ferrite. Through SEM imagines, it can be found that samples had spherical cube shapes. The binding energy peaks of Ni, Mg, Zn, Fe and O were discovered by XPS technique, which are main elements related to this experiment. The sample prepared with EDTA had better magnetic properties, Ms is 38.25 emu/g, Mr is 1.8003 emu/g and Hc is 12.027 Oe. It has excellent characteristics as a soft magnetic material and possesses a broad development prospect on magnetic recording applications.

## Author contributions

Yanchun Zhang: contributed to experiment, conceptualization, investigation, writing-original draft and visualization; Aimin Sun: checked the manuscript; Nanzhaxi Suo: helped in measurement of data, experimental process, checking the figure.

## Additional Information

Competing financial interests: The authors declare no competing financial interests.
Supplementary information: The authors claim that none of the material in the paper has been published or is under consideration for publication elsewhere.

## References


[1] Mathew George, Asha Mary Johna, Swapna S. Nair, P.A. Joy, M.R. Anantharaman. Finite size effects on the structural and magnetic properties of sol-gel synthesized $NiFe_2O_4$ powders. J. Magn. Magn. Mater. 302 (2006) 190–195.

[2] K. Maaz et al. Structural analysis of nickel doped cobalt ferrite nanoparticles prepared by coprecipitation route. Phys. B 404 (2009) 3947–3951.

[3] Sasanka Deka and P. A. Joy. Enhanced Permeability and Dielectric Constant of Ni-Zn Ferrite Synthesized in Nanocrystalline Form by a Combustion Method. J. Am. Ceram. Soc., 90 [5] 1494–1499 (2007).

[4] R.C. Kambale, N.R. Adhate, B.K. Chougule, Y.D. Kolekar. Magnetic and dielectric properties of mixed spinel Ni–Zn ferrites synthesized by citrate–nitrate combustion method. J. Alloy. Compd. 491 (2010) 372–377.

[5] Chaocheng Liu, Xucai Kan, Xiansong Liu, Zhitao Zhang and Jiyu Hu. Magnetic compensation and critical behavior in spinel $Co_2TiO_4$. Phys. Chem. Chem. Phys.

[6] Wei Yang, Xucai Kan, Xiansong Liu, Zhongzhu Wang, Zuhua Chen, Zhen Wang, Ruiwei Zhu, Mudssir Shezad. Spin glass behavior in $Zn_{0.8-x}Ni_xCu_{0.2}Fe_2O_4$ ($0 \leqq x \leqq 0.28$) ferrites. Ceram. Int. 45 (2019) 23328-23332.

[7] Yong Li, Xucai Kan, Xiansong Liu, Shuangjiu Feng, Qingrong Lv, Khalid Mehmood Ur Rehma, Wei Wang, Chaocheng Liu, Xiaohui Wang, Yuliang Xu. Spin-glass evolution behavior in spinel compounds $Co_{2-x}Zn_xSnO_4$ ($0 \leqq x \leqq 1$). J. Alloy. Compd.

[8] J.Topfer, H.Kahnt, P.Nauber, S.Senz, D.Hesse. Microstructural effects in low loss power ferrites. J. European Ceram.Soc. 25 (2005) 3045–3049.

[9] Jun-Gang Hou, Yuan-Fang Qu, Wei-Bing Ma, Qing-Chi Sun. Effect of $CuO–Bi_2O_3$ on low temperature sintered MnZn-ferrite by sol–gel auto-combustion method. J. Sol-Gel Sci Technol. (2007) 44:15‑20.

[10] Urvi V. Chhaya, Bimal S. Trivedi and R.G. Kulkarni. Magnetic properties of the mixed spinel $NiAl_xCr_xFe_{2-2x}O_4$. Hyperfine Interact. 116 (1998) 197‑207.

[11] Manish Srivastava, Animesh K. Ojha , S. Chaubeya, Prashant K. Sharma, Avinash C. Pandey. Inflfluence of pH on structural morphology and magnetic properties of ordered phase cobalt doped lithium ferrites nanoparticles synthesized by sol–gel method. Mater. Sci. Eng. B 175 (2010) 14–21.

[12] Yingqiang Han, Aimin Sun, Xiaoguang Pan, Wei Zhang, Xiqian Zhao. Effect of Different Sintering Temperatures on Structural and Magnetic Properties of Zn–Co Ferrite Nanoparticles. J. Supercond. Nov.Magn.

[13] Chunxiang Cao , Ailin Xia , Shunkai Liu ,Liuniu Tong. Synthesis and magnetic properties of hydrothermal magnesium-zinc spinel ferrite powders. J Mater Sci: Mater Electron (2013) 24:4901–4905.

[14] P. Raju , S. R. Murthy. Preparation and characterization of Ni–Zn ferrite + polymer nanocomposites using mechanical milling method. Appl Nanosci (2013) 3:469‑475.

[15] U. V. CHHAYA, B. S. TRIVEDI, R. G. KULKARNI, Magnetic ordering and properties of nickel ferrite doped with $Al^{3+}$ and $Cr^{3+}$ ions. J. Mater. Sci. Lett. 18 (1999 ) 1177 – 1179.

[16] D.H. Bobade, S.M. Rathod, Maheshkumar L. Mane, Sol-gel auto-combustion synthesis, structural and enhanced magnetic properties of $Ni^{2+}$ substituted nanocrystalline Mg-Zn spinel ferrite. Phys. B 407 (2012) 3700-3704.

[17] Montana Sangmanee, Santi Maensiri. Nanostructures and magnetic properties of cobalt ferrite ($CoFe_2O_4$) fabricated by electrospinning. Appl. Phys. A (2009) 97: 167–177.

[18] Yu¨ksel Koseoglua,n , Mousa Ibrahim Oleiwi Oleiwia , Resul Yilginb , Abdullah N. Kocbay. Effect of chromium addition on the structural, morphological and magnetic properties of nano-crystalline cobalt ferrite system. Ceram. Int. 38 (2012) 6671–6676.

[19] K. Maaz, W. Khalid, A. Mumtaz, S.K. Hasanain, J. Liu, J.L. Duan. Magnetic characterization of $Co_{1-x}Ni_xFe_2O_4$ nanoparticles prepared by co-precipitation route. Phys. E 41 (2009) 593–599.

[20] Dong Wang , Jun Zhou , Xi Zhou , Xue-bin Ke , Chuan Chen , Ya-run Wang , Yong-liang Liu , Lei Ren. Facile ultrafast microwave synthesis of monodisperse $MFe_2O_4$ (M=Fe, Mn, Co, Ni) superparamagnetic nanocrystals. Mater. Lett. 136 (2014) 401–403.

[21] Jiang jing, Li Liangchao, Xu Feng. Structural analysis and magnetic properties of Gd-doped Li-Ni ferrites prepared using rheological phase reaction method. J. Rare Earths 25 (2007) 79-83.

[22] S. Karimi, P. Kameli , H. Ahmadvand, H. Salamati. Effects of Zn-Cr-substitution on the structural and magnetic properties of Ni1-xZnxFe2-xCrxO4 ferrites. Ceram. Int. 42 (2016) 16948–16955.

[23] K. Siraj , M. Khaleeq-ur-Rahman, S.I. Hussain, M.S. Rafifique, S. Anjum.Effect of deposition temperature on structural, surface, optical and magnetic properties of pulsed laser deposited Al-doped CdO thin films. J. Alloy. Compd.509 (2011) 6756–6762.

[24] V.Pillai, D.O. Shah.Synthesis of high-coercivity cobalt ferrite particles using water-in-oil microemulsions. J. Magn. Magn. Mater.163 (1996) 243-248.

[25] M. A. Cobos, P. de la Presa,I. Llorente J. M. Alonso,A. García-Escorial,P. Marín, A. Hernando,and J. A. Jimenez. Magnetic Phase Diagram of Nanostructured Zinc Ferrite as a Function of Inversion Degree δ. : J. Phys. Chem. C 2019, 123, 17472−17482.

[26] M.A. Gabal, Reda M. El-Shishtawy, Y.M. Al Angari. Structural and magnetic properties of nano-crystalline Ni-Zn ferrites synthesized using egg-white precursor. J. Magn. Magn. Mater. 324 (2012) 2258–2264.

[27] C. Choodamani, G.P. Nagabhushana, B. Rudraswamy, G.T. Chandrappa. Thermal effect on magnetic properties of Mg-Zn ferrite nanoparticles. Mater. Lett. 116 (2014) 227–230.

[28] Shaban I. Hussein, Ashraf S. Elkady, M.M. Rashad, A.G. Mostafa, R.M. Megahid. Structural and magnetic properties of magnesium ferrite nanoparticles prepared via EDTA-based sol-gel reaction. J.Magn. Magn. Mater. 379 (2015) 9–15

[29] G. M. BHONGALE, D. K. KULKARNI and V. B. S. SAPRE, New formula for lattice dimension of an oxide spinel with cubic structure. Bull. Mater. Sci. 15, 121-125 (1992).

[30] N. Sharma, P. Aghamkar, S. Kumar, M. Bansal, R.P.Tondon Anji, Study of structural and magnetic properties of Nd doped zinc ferrites. J. Magn. Magn. Mater.369 (2014), 162–167.

[31] Dinesh Kumar, Abhishek Kumar, Rajiv Prakash and Akhilesh Kumar Singh. X-ray Diffraction Analysis of $Cu^{2+}$ Doped $Zn_{1-x}Cu_xFe_2O_4$ Spinel Nanoparticles using Williamson-Hall Plot Method. Advances in Basic Science (ICABS 2019).

[32] Siraj, K., Khaleeq-ur-Rahman, M., Hussain, S.I., Rafique, M.S., Anjum, S.: Effect of deposition temperature on structural, surface, optical and magnetic properties of pulsed laser deposited Al-doped CdO thin films. J. Alloy. Compd. 509, 6756–6762 (2011).

[33] B. D. Cullity, J. W. Weymouth.: Elements of X-Ray Diffraction. American Journal of Physics 25, 394 (1957).

[34] Wei Zhang , Aimin Sun, Xiqian Zhao , Xiaoguang Pan , Yingqiang Han , Nanzhaxi Suo , Lichao Yu , Zhuo Zuo. Structural and magnetic properties of Ni-Cu-Co ferrites prepared from sol-gel auto combustion method with different complexing agents. J. Alloy. Compd. 816 (2020) 152501.

[35] R. D. Waldron. Infrared Spectra of Ferrites. Phys.Rev. 99 (1955) 1727.

[36] K.H. Wu, T.H. Ting, C.C. Yang, G.P.Wang. Effect of complexant/fuel on the chemical and electromagnetic properties of $SiO_2$-doped Ni-Zn ferrite. Materials Science and Engineering B 123 (2005) 227–233.

[37] Sonia Gaba, Ashok Kumar, Pawan S. Rana, J. Supercond. Nov. Magn. (2018).

[38] V.K. Mittal, Santanu Bera, R. Nithya, M.P. Srinivasan, S. Velmurugan, S.V. Narasimhan. Solid state synthesis of Mg-Ni ferrite and characterization by XRD and XPS. J. Nuclear Mater. 335 (2004) 302-310.

[39] Pratibha Rao, Rajeev C. Chikateb and Sunita Bhagwat. Highly responsive and stable Y3+ doped NiMg–ferrite thick films as an efficient humidity sensor. New J. Chem.

[40] Shurong Wang, Jingxv Zhang, Jiedi Yang, Xueling Gao, Hongxin Zhang,Yanshuang Wang and Zhenyu Zhu. Spinel ZnFe2O4 nanoparticle-decorated rod-like ZnO nanoheterostructures for enhanced gas sensing performances. RSC Adv., 2015, 5, 10048.

[41] U.B. Gawas, V.M.S. Verenkar, S.R. Barman, S.S. Meena, Pramod Bhatt. Synthesis of nanosize and sintered $Mn_{0.3}Ni_{0.3}Zn_{0.4}Fe_2O_4$ ferrite and their structural and dielectric studies. J. Alloy. Compd.555 (2013) 225-231.

[42] Lexi Zhang, Jianghong Zhao, Haiqiang Lua, Liming Gong, Li Li, Jianfeng Zheng, Hui Li, Zhenping Zhu. High sensitive and selective formaldehyde sensors based on nanoparticle-assembled ZnO micro-octahedrons synthesized by homogeneous precipitation method. Sensors and Actuators B 160 (2011) 364-370.

[43] Wei Zhang, Aimin Suna, Xiaoguang Pan, Yingqiang Han, Xiqian Zhao, Lichao Yu, Zhuo Zuo, Nanzhaxi Suo. Magnetic transformation of Zn-substituted Mg-Co ferrite nanoparticles: Hard magnetism→soft magnetism. J. Magn. Magn. Mater. 506 (2020) 166623.

[44] Li Wang, Ji Li, Ming Lu, He Dong, Jie Hua, Shichong Xu, Haibo Li. Magnetic and Mossbauer Spectroscopy Studies of NiFe2O4/SiO2 Nanocomposites Synthesized by Sol-Gel Method. J Supercond Nov Magn.

[45] A. Franco, Jr and M. S. Silva. High temperature magnetic properties of magnesium ferrite nanoparticles. Journal Of Applied Physics 109, 07B505 (2011).

[46] Xiqian Zhao, Aimin Sun, Wei Zhang, Lichao Yu, Zhuo Zuo, Nanzhaxi Suo, Xiaoguang Pan, Yingqiang Han. Magnetic transformation of Zn‑substituted Ni‑Co ferrite nanoparticles. Journal of Materials Science: Materials in Electronics (2020) 31:526‑541.

[47] K.B. Modi, J.D. Gajera, M.C. Chhantbar, K.G. Saija, G.J. Baldha, H.H. Joshi. Structural properties of magnesium and aluminium co-substituted lithium ferrite. Materials Letters 57 (2003) 4049-4053.

[48] Chandra Babu Naidu K., Madhuri W. Microwave assisted solid state reaction method: Investigations on electrical and magnetic properties NiMgZn ferrites. Mater. Chem.Phys. 181 (2016) 432-443.

[49] R.H. Kadam, A.P. Birajdar , Suresh T. Alone , Sagar E. Shirsath Fabrication of $Co_{0.5}Ni_{0.5}Cr_xFe_{2x}O_4$ materials via sol–gel method and their characterizations. J. Magn. Magn. Mater.327 (2013) 167–171.

[50] S. Singhal, K. Chandra. Cation distribution and magnetic properties in chromium-substituted nickel ferrites prepared using aerosol route. J. Solid State Chem. 180 (2007) 296–300.

[51] P.A. Shaikh et al. Effect of Ni doping on structural and magnetic properties of $Co_{1-x}Ni_xFe_{1.9}Mn_{0.1}O_4$. J. Magn. Magn. Mater. 322 (2010) 718–726.

[52] Nanzhaxi Suo, Aimin Sun, Lichao Yu· Zhuo Zuo, Xiqian Zhao, Wei Zhang, Yanchun Zhang, Liqiong Shao, Tengxuan Yu. Preparation and study of lattice structure and magnetic properties of $Bi^{3+}$ ion-doped Ni-Mg-Co ferrites by sol-gel auto-combustion method. J. Sol-Gel Sci. Technol.

[53] I. Panneer Muthuselvam, R.N. Bhowmik. J. Magn. Magn. Mater. 322 (2010) 767–776.

[54] J. Judith Vijaya, et al., Effect of $Cu^{2+}$ doping on structural, morphological, optical and magnetic properties of MnFe2O4 particles/sheets/flakes-like nanostructures, Ceramics International (2013).

[55] R. Saranya, R. Azhagu Raj, M. S. AlSalhi, S. Devanesan. Dependence of Catalytic Activity of Nanocrystalline Nickel Ferrite on Its Structural, Morphological, Optical, and Magnetic Properties in Aerobic Oxidation of Benzyl Alcohol. J Supercond Nov Magn.

[56] H. Harzali, A. Marzouki, F. Saida, A. Megriche, A. Mgaidi, Structural, magnetic and optical properties of nanosized $Ni_{0.4}Cu_{0.2}Zn_{0.4}R_{0.05}Fe_{1.95}O_4$ (R=Eu3+, Sm3+, Gd3+ and Pr3+) ferrites synthesized by co-precipitation method with ultrasound irradiation, Journal of Magnetism and Magnetic Materials (2018).

[57] T.M. Hammad, J.K. Salem, A.A. Amsha, N.K. Hejazy, Optical and magnetic characterizations of zinc substituted copper ferrite synthesized by a co-precipitation chemical method, Journal of Alloys and Compounds (2018), doi: 10.1016/j.jallcom.2018.01.123.

[58] Adel Maher Wahba, Mohamed Bakr Mohamed and N.G. Imam, Correlating structural, magnetic, and luminescence properties with the cation distribution of $Co_{0.5}Zn_{0.5+x}Fe_{2-x}O_4$ nanoferrite, Journal of Magnetism and Magnetic Materials.

# Figures

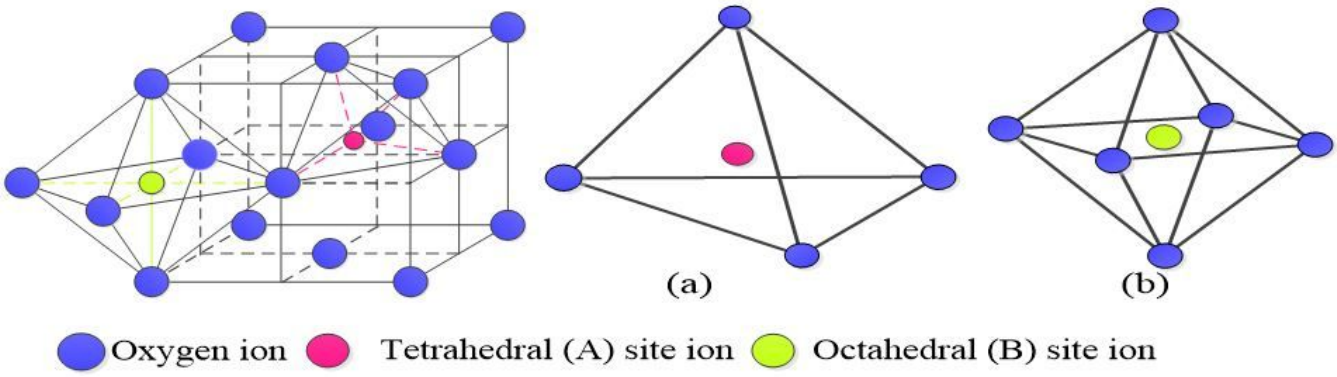


**Figure 1**

The crystal structure of spinel ferrite and the distribution of metal cations and oxygen ions. (a) Tetrahedral (A) site; (b) Octahedral (B) site.

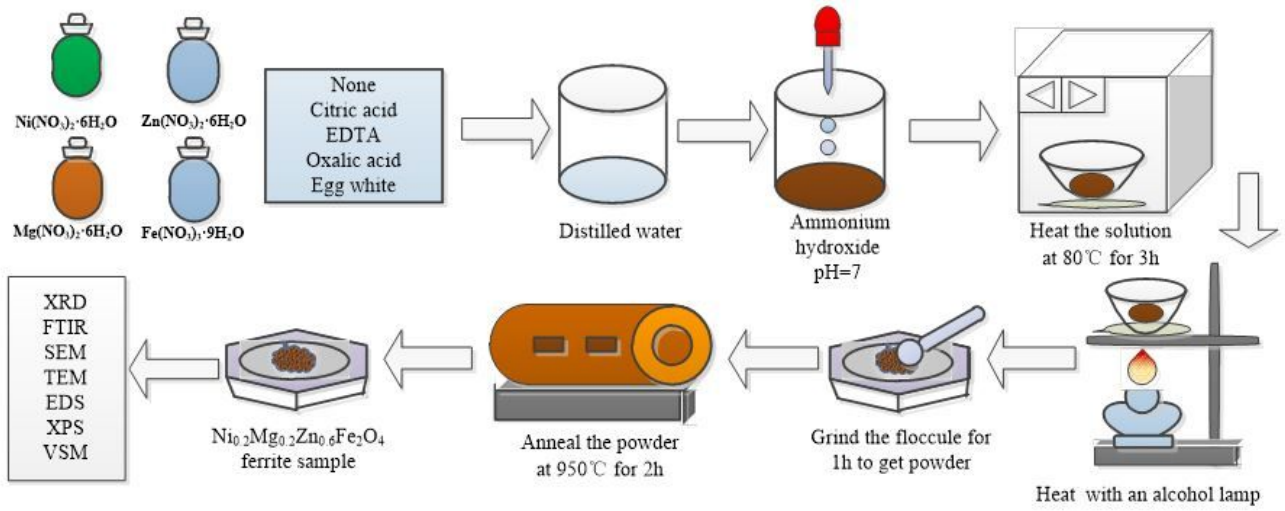


**Figure 2**

The flow chart of preparing Ni0.2Mg0.2Zn0.6Fe2O4 nano ferrite with different complexing agents by sol-gel method.

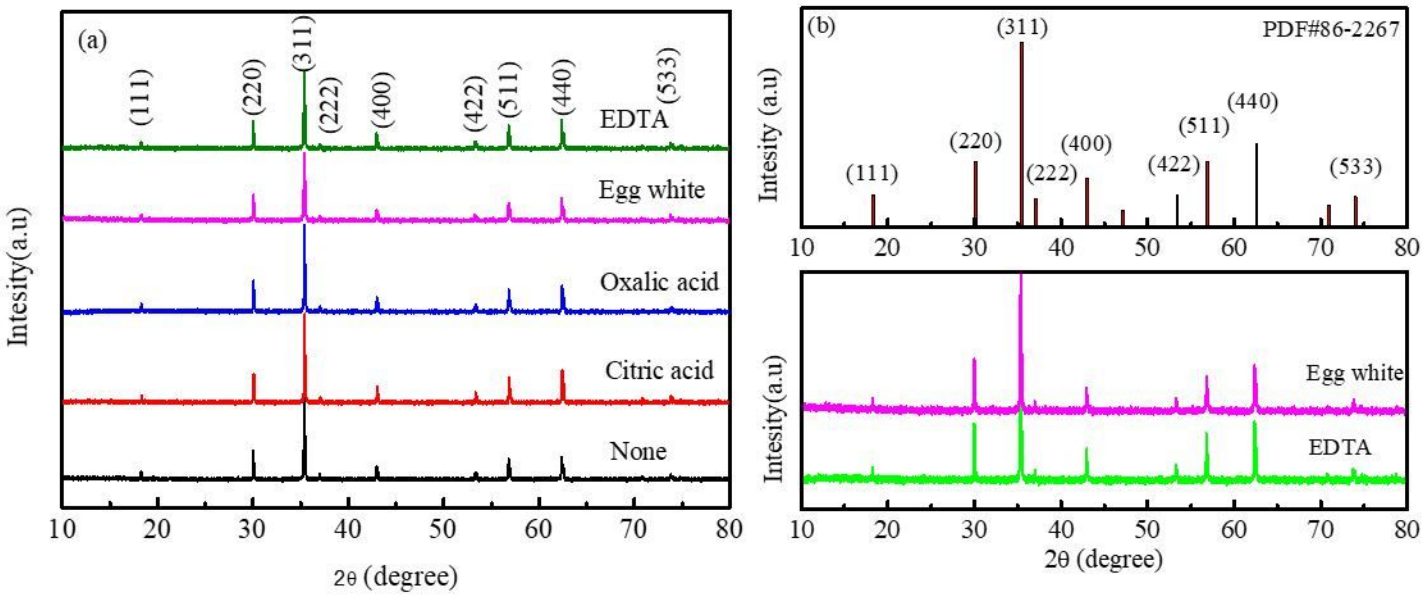


## Figure 3

(a) shows the X-ray diffraction pattern of Ni0.2Mg0.2Zn0.6Fe2O4 nano ferrite prepared with different complexing agents, (b) shows the XRD pattern of samples with egg white and EDTA as complexing agent contrasting with JCPDS card # 86-2267.

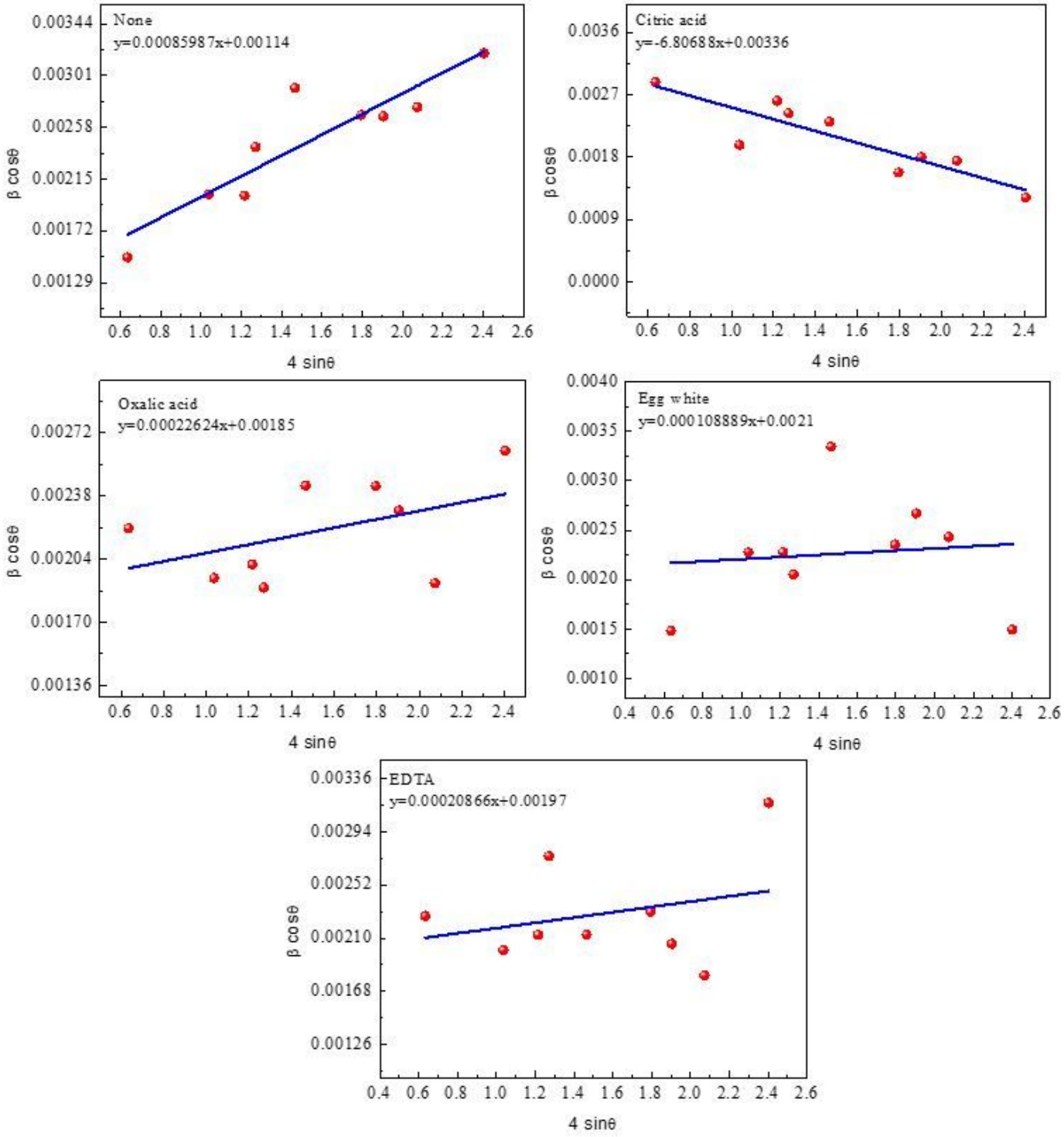


## Figure 4

Williamson-Hall plots of Ni0.2Mg0.2Zn0.6Fe2O4 nano ferrite prepared with different complexing agents.

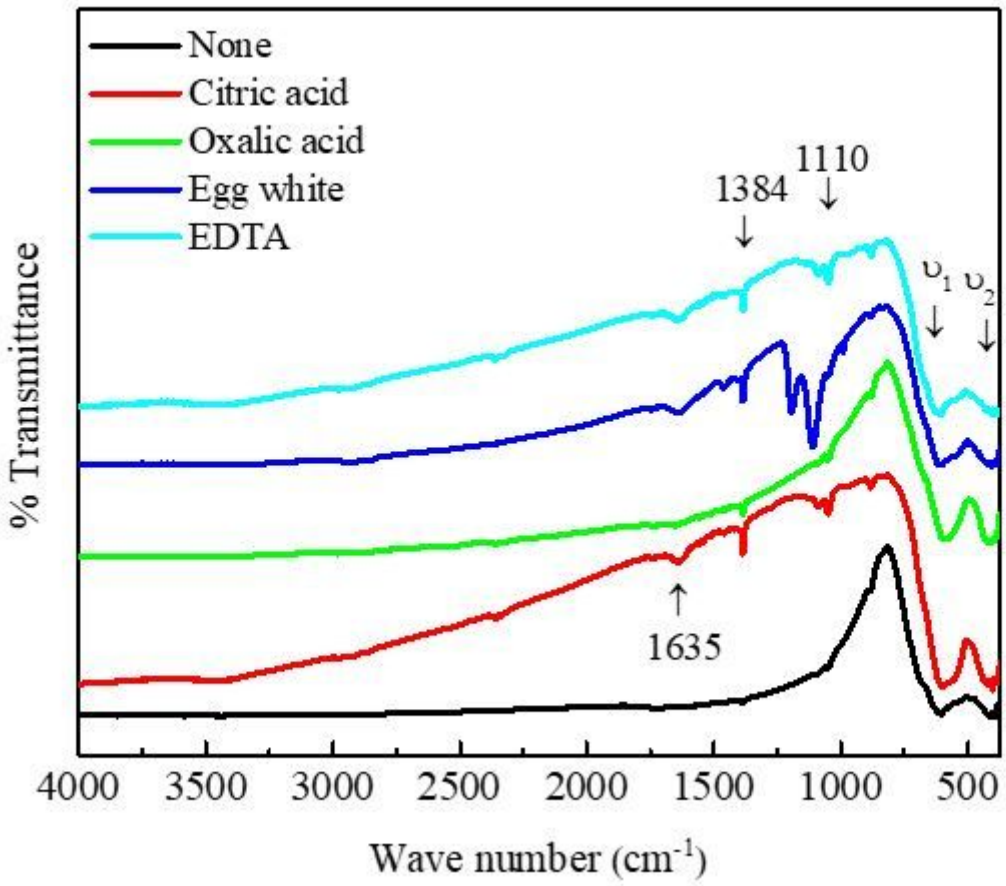


**Figure 5**

FTIR spectra of Ni0.2Mg0.2Zn0.6Fe2O4 nano ferrite prepared with different complexing agents.

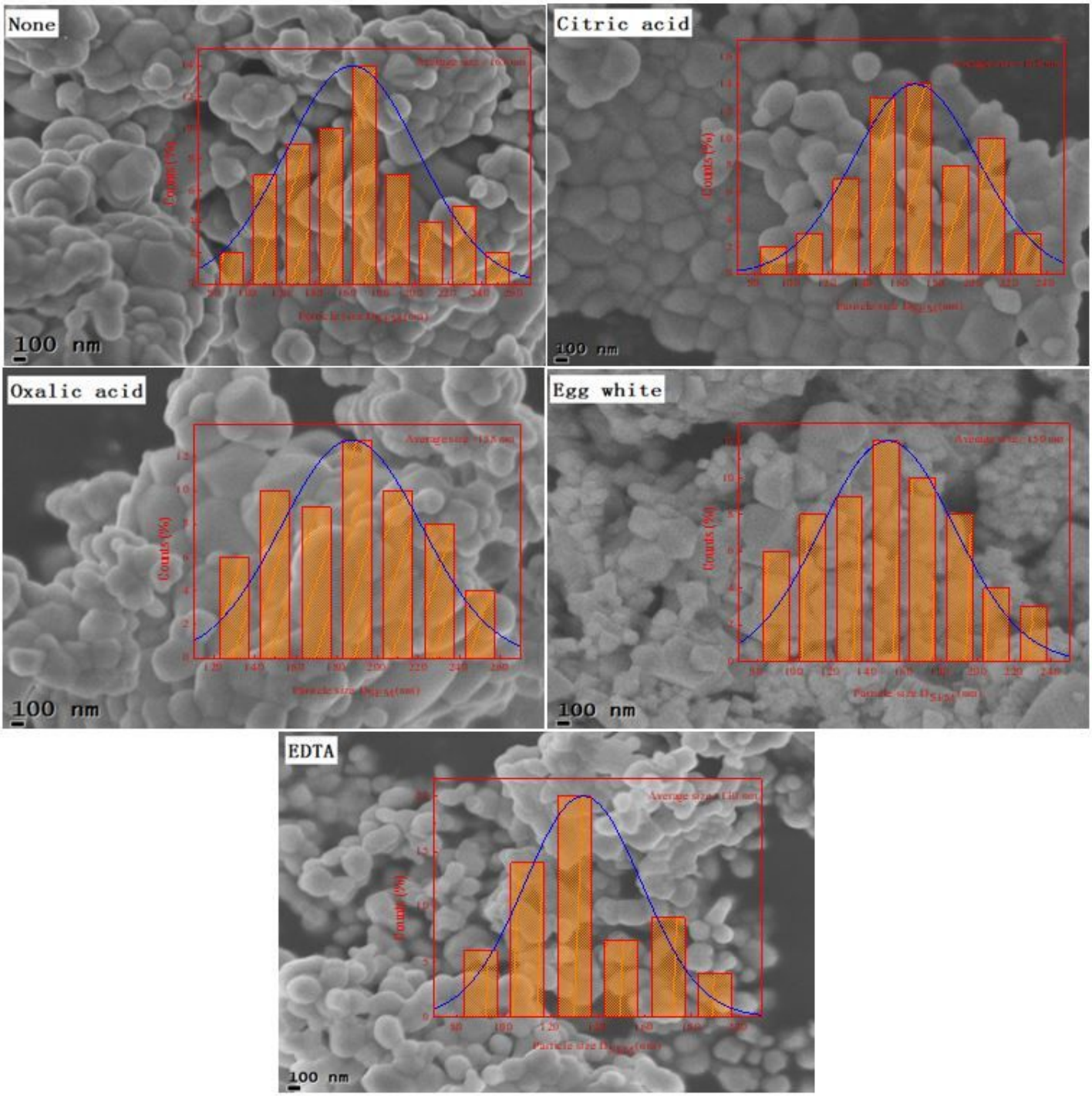


## Figure 6

SEM micrographs and particles size distribution histograms of Ni0.2Mg0.2Zn0.6Fe2O4 nano ferrite prepared with different complexing agents.

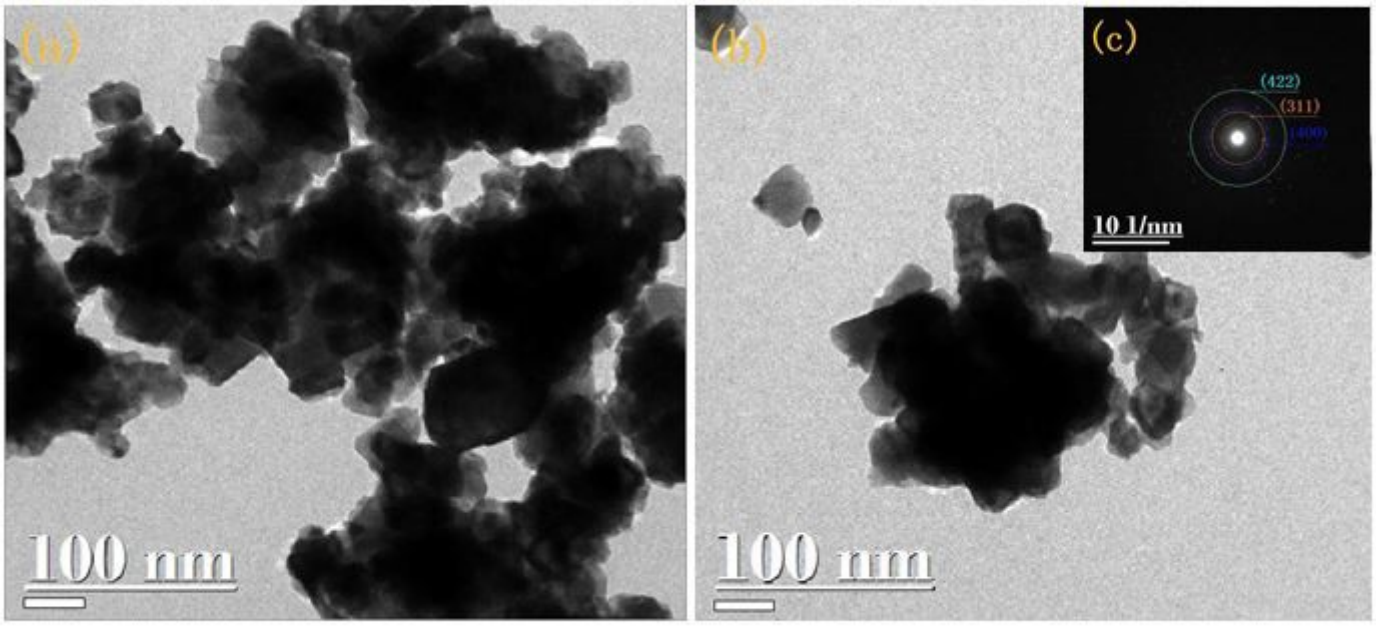


**Figure 7**

TEM images and the SAED of Ni0.2Mg0.2Zn0.6Fe2O4 nano ferrite particles prepared with EDTA.

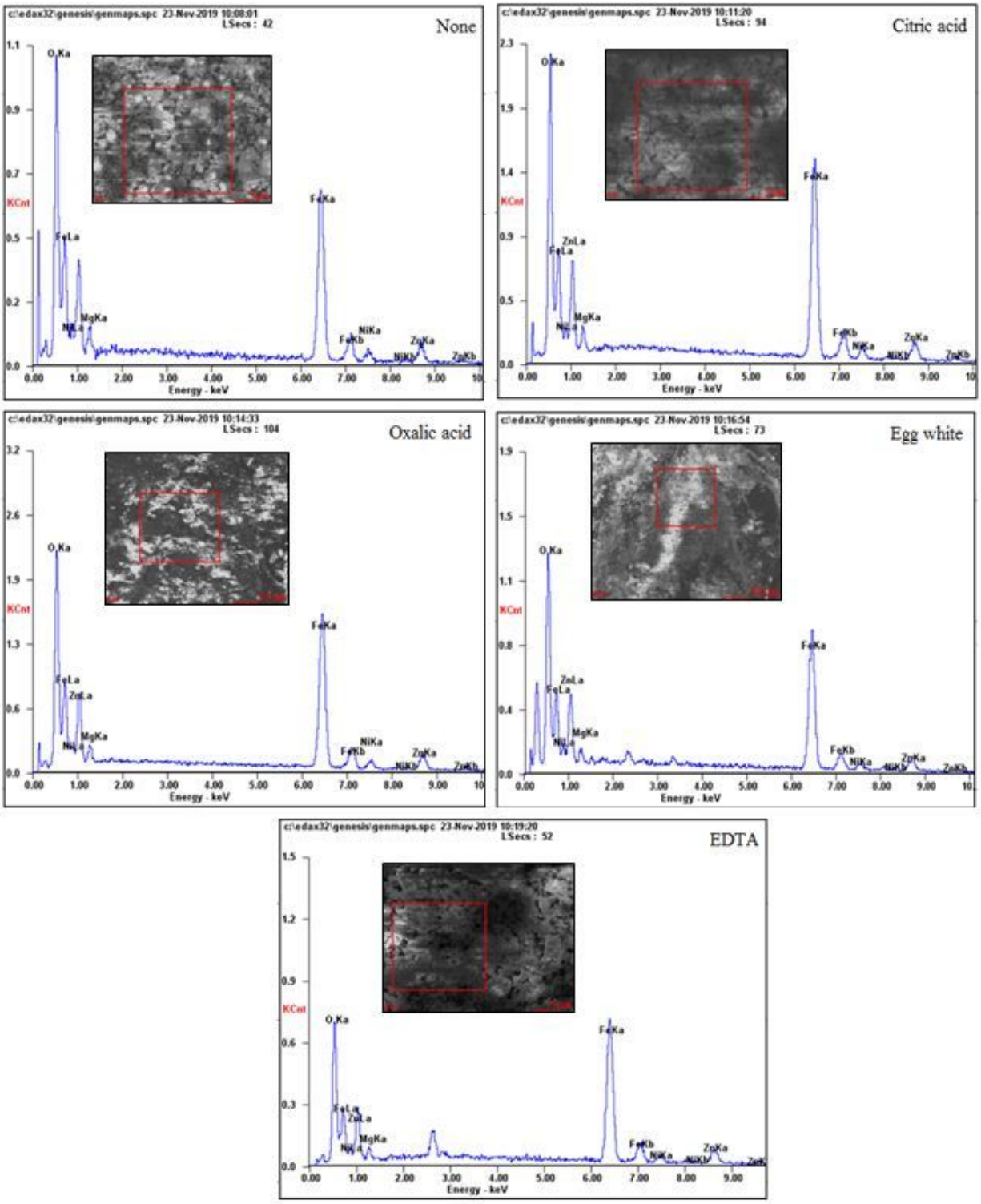


## Figure 8

The EDS diagrams of Ni0.2Mg0.2Zn0.6Fe2O4 nano ferrite prepared with different complexing agents.

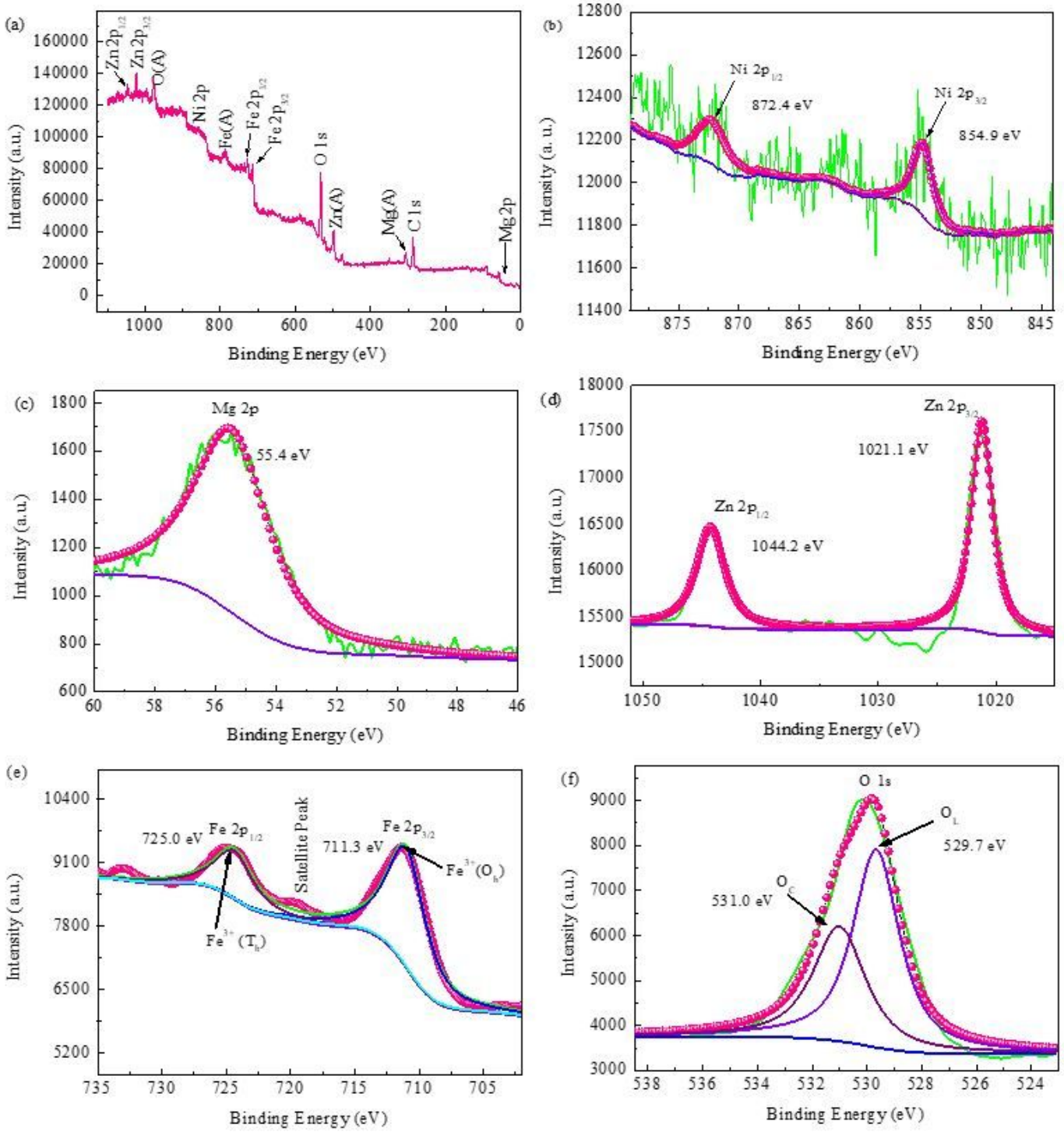


## Figure 9

X-ray photoelectron spectra (XPS) of Ni0.2Mg0.2Zn0.6Fe2O4 nano ferrite prepared using EDTA as complexing agents. (a) survey spectrum and high-resolution spectra for (b) Ni 2p, (c) Mg 2p, (d) Zn 2p, (e) Fe 2p, (f) O 1s.

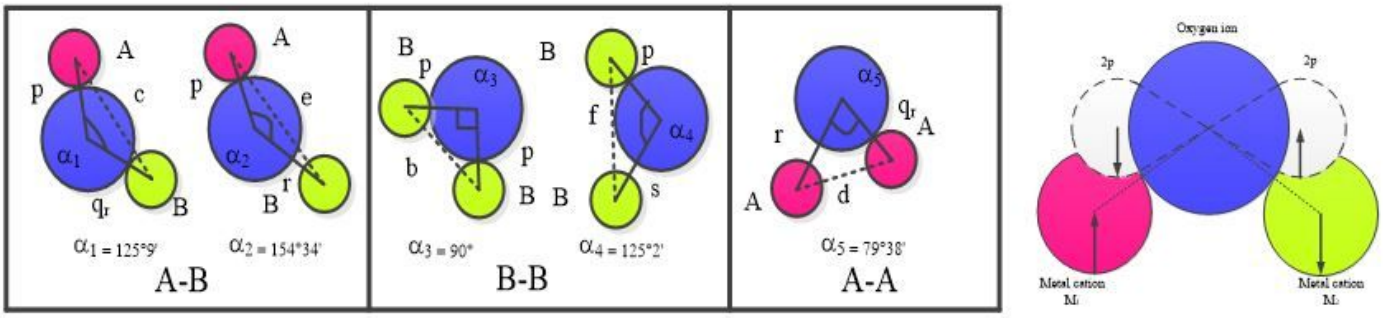


## Figure 10

The relative positions of metal ions and oxygen ions in the superexchange of spinel ferrite.

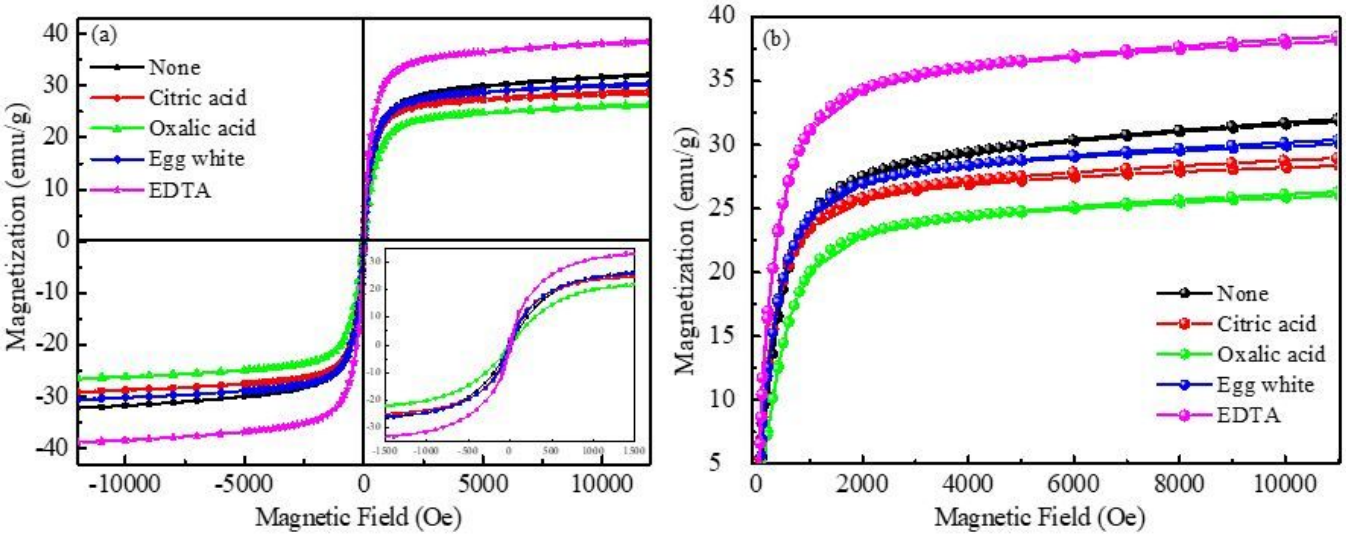


## Figure 11

(a) shows M-H Hysteresis loops of Ni0.2Mg0.2Zn0.6Fe2O4 nano ferrite prepared with different complexing agents, (b) shows a larger view of the first quadrant in hysteresis loops.

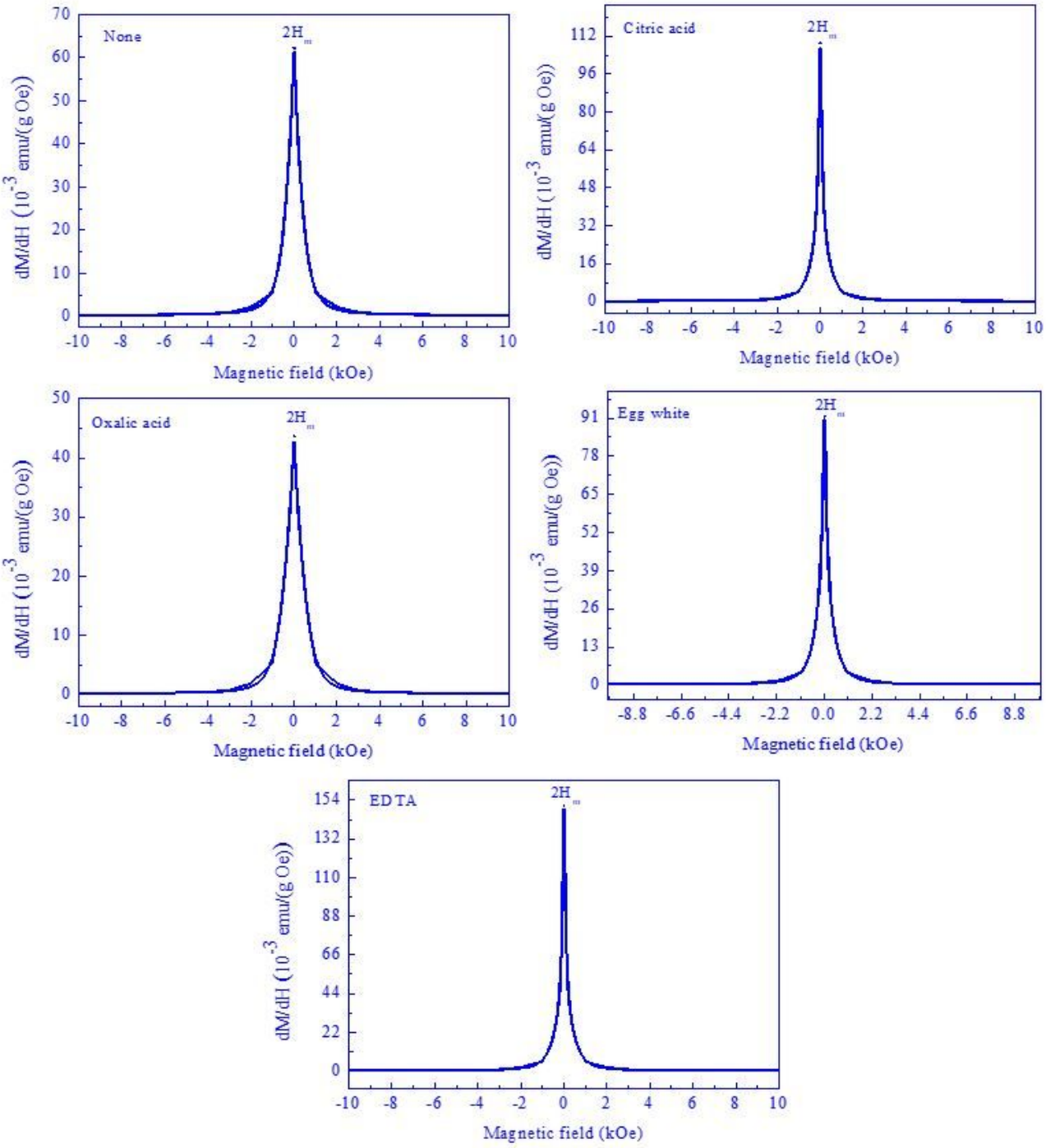


## Figure 12

Field dependence of dM/dH of samples prepared with different complexing agents. 2Hm measures the magnetic field that separates two peaks.

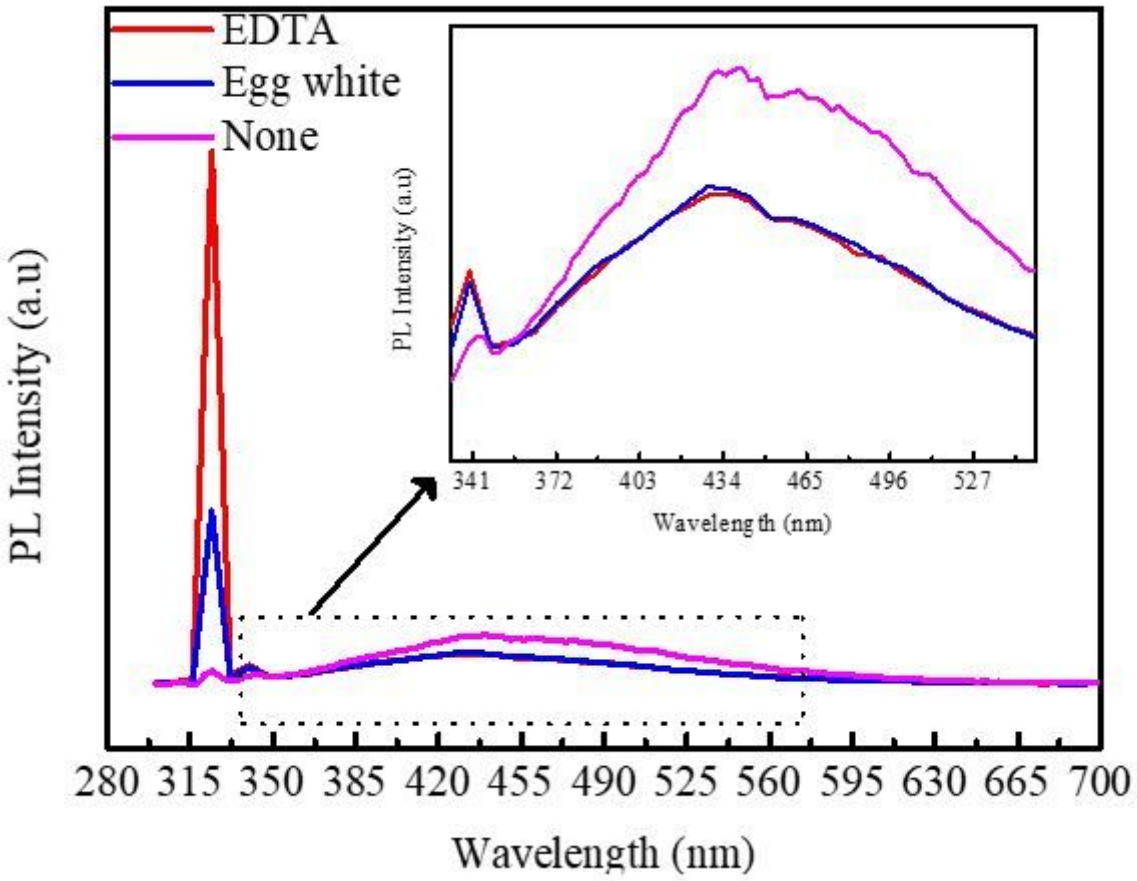


**Figure 13**

PL spectra of Ni0.2Mg0.2Zn0.6Fe2O4 nano ferrite prepared with none, egg white and EDTA as complexing agents.

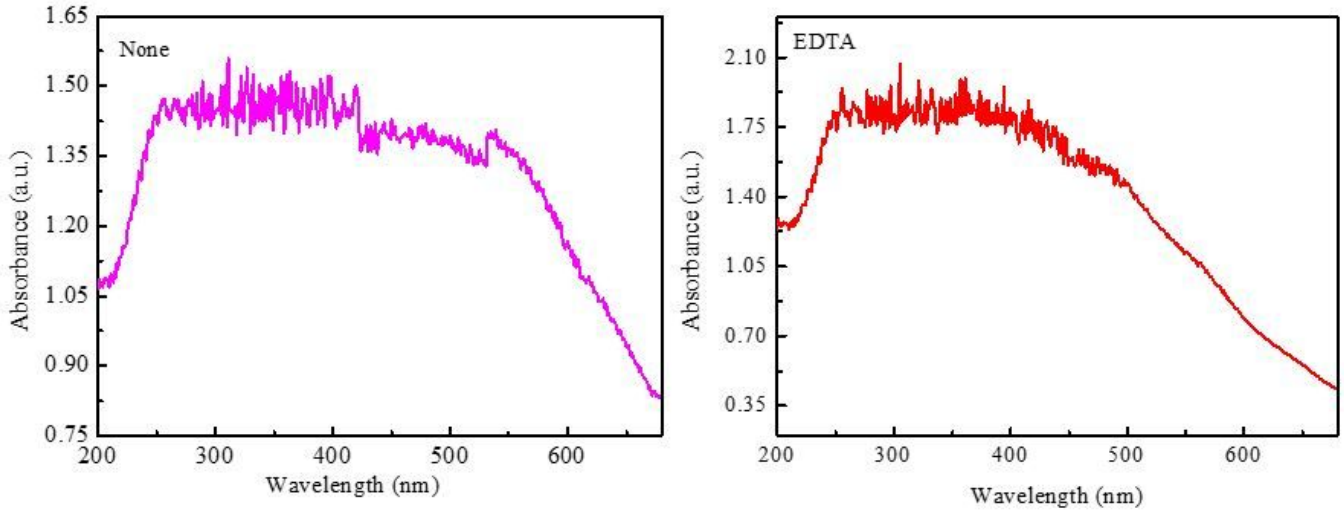


**Figure 14**

UV-Vis absorption spectrum of Ni0.2Mg0.2Zn0.6Fe2O4 nano ferrite prepared with none and EDTA as complexing agents.

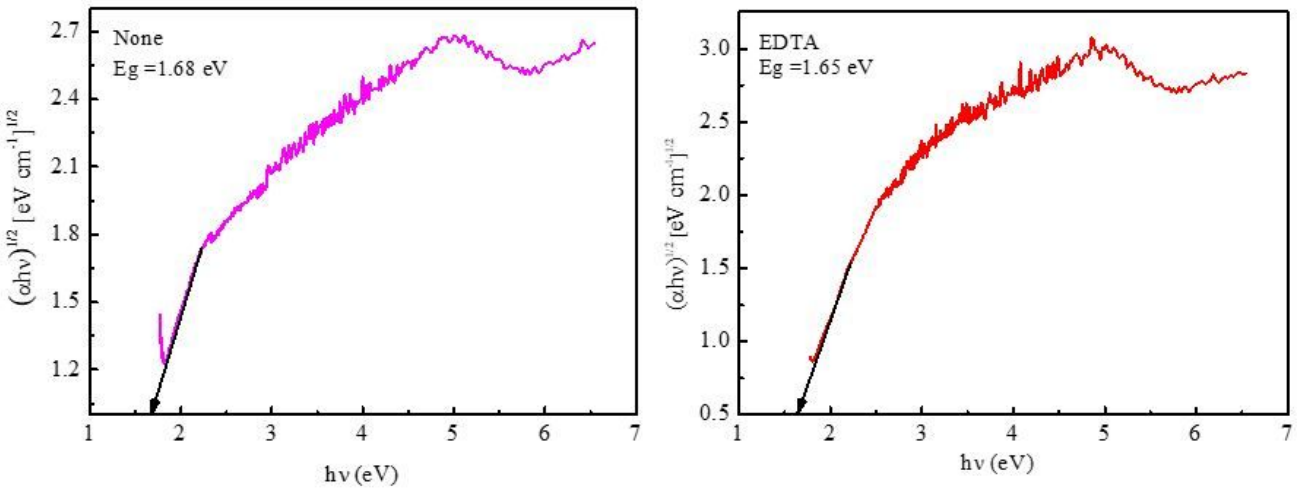


**Figure 15**

Tauc plots of Ni0.2Mg0.2Zn0.6Fe2O4 nano ferrite prepared with none and EDTA as complexing agents.